PASJ: Publ. Astron. Soc. Japan , 1–**??**,

Dynamical Effects of CDM Subhalos on a Galactic Disk

Hirohito Hayashi and Masashi Chiba
Astronomical Institute, Tohoku University, Sendai 980-8578
hayashi@astr.tohoku.ac.jp, chiba@astr.tohoku.ac.jp

(Received ; accepted)

Abstract

We investigate the dynamical interaction between a galactic disk and surrounding numerous dark subhalos as expected for a galaxy-sized halo in the cold dark matter (CDM) models. Our particular interest is to what extent accretion events of subhalos into a disk are allowed in light of the observed thinness of a disk. Several models of subhalos are considered in terms of their internal density distribution, mass function, and spatial and velocity distributions. Based on a series of N-body simulations, we find that the disk thickening quantified by the change of its scale height, Δz_d, depends strongly on the individual mass of an interacting subhalo $M_{\rm sub}$. This is described by the relation, $\Delta z_d/R_d \simeq 8\sum_{j=1}^{N}(M_{{\rm sub},j}/M_d)^2$, where R_d is a disk scale length, M_d is a disk mass, and N is the total number of accretion events of subhalos inside a disk region ($\leq 3R_d$). Using this relation, we find that an observed thin disk has not ever interacted with subhalos with the total mass of more than 15 % disk mass. Also, a less massive disk with smaller circular velocity V_c is more affected by subhalos than a disk with larger V_c, in agreement with the observation. Further implications of our results for the origin of a thick disk component are also discussed.

Key words: cosmology: dark matter — galaxies: formation — galaxies: structure — galaxies: interactions

1. Introduction

The cold dark matter (CDM) paradigm has become a standard framework for understanding the structure formation in the Universe. According to this theoretical paradigm, the growing process of self-gravitating structures is hierarchical in the sense that small dark matter halos virialize first, and aggregate successively into larger and larger objects. This clustering process of dark matter halos is successful for explaining a wide variety of observations including the large-scale distribution of galaxies.

In this CDM scenario, N-body simulations are an important tool in order to investigate the non-linear growth of cosmological structures. Early N-body simulations based on the CDM models suffered from the so-called *over-merging* problem, i.e., substructures are disrupted very quickly within dense environments (Summers et al. 1995). However, recent high-resolution N-body simulations have revealed the presence of hundreds of dark matter substructures (subhalos) which survive in not only cluster scales but also galactic scales (Moore et al. 1999; Klypin et al. 1999). This large number of subhalos in a galaxy-sized halo is in contrast to only about a dozen satellite galaxies in the Galaxy, which confronts so-called "the Missing Satellite Problem". Several authors have argued that this apparent discrepancy could be resolved by considering some suppressing process for star formation, such as gas heating by an intergalactic ionizing background or energy feedback from evolving stars. In whatever models relying on the suppression of galaxy formation, a typical galaxy-sized halo should contain numerous dark subhalos.

Then, there is a possibility that a large amount of subhalos interact frequently with a stellar disk embedded in the center of a halo, so that the disk would be dynamically heated and thickened. On the other hand, an observed galactic disk is rather thin: the scale height (or half thickness) is only about ~ 250 pc in the Galaxy. Likewise, recent observations of external disk galaxies (Kregel et al. 2002) suggest that the observed scale height of a disk, z_d, is confined to some limiting value relative to the scale length of a disk, R_d, i.e, $z_d/R_d < 0.2$.

This observed thinness of a disk provides important limits on the disk heating due to infalling satellites. Tóth & Ostriker (1992) analytically evaluated this effect and concluded that an observed disk like that of the Galaxy within the solar radius should have interacted with satellites with no more than 4 % of the present disk mass within the last 5 Gyr. Subsequent numerical simulations of an interaction between a disk and a single satellite (e.g. Velázquez & White 1999) showed that their analytical estimation for the disk heating was somewhat too high because an actual interaction process is highly non-linear and more complicated than simplified analytical representation. Interactions with many subhalos would be much more complicated and thus require a more detailed analysis.

Font et al. (2001) have conducted numerical simulation of interaction between a disk and numerous subhalos based on the CDM models. They concluded that the effect of subhalos on a disk is rather small, and therefore subhalos do not conflict with the presence of a thin disk since their orbit seldom take them near the disk. However, it is worth noting that in their simulation the initial scale height of a disk (700 pc) is already thick compared with the observed one in the Galaxy (~ 250 pc), thereby leading to possibly the underestimation of the disk heating effect. Their simulation is also limited to only one realization of subhalos; it is yet unclear whether the derived weak effect of subhalos on a disk is general or not. Ardi et al. (2003) have investigated more details in this disk heating by subhalos. They found that a more massive subhalo is more effective to heat the disk than a less massive one. However, in their calculation subhalos are represented by rigid bodies which never lose their mass irrespective of tidal effects of a host galaxy, so that the disk heating is overestimated. Also, the applicability of their result to an actual disk, especially, to what extent accretion events of subhalos into a disk are allowed remains unclear.

Our aim in this paper is thus to set more useful limits on the dynamical interaction between numerous subhalos and a galactic disk. For this purpose, we conduct a series of numerical simulations, in which a self-gravitating disk is embedded in a dark halo containing many subhalos. In this work we set an initially thin disk with the scale height of 250 pc, in contrast to previous numerical studies starting from the scale height of ~ 700 pc much larger than the observed one (Velázquez & White 1999; Font et al. 2001). Several models for the system of subhalos in a host halo are taken into account in terms of their mass function, spatial distribution, and velocity distribution. We also consider two different models for the internal density distribution of subhalos: point-mass and extended-mass models. In the latter model, subhalos are affected by a tidal field of a host galaxy so that they lose their mass in the course of their orbital motions. Based on our simulations, we investigate the dependence of the disk heating on the model parameters and apply our analysis to understanding an observed thin disk in the context of the disk heating by subhalos.

This paper is organized as follows. In § 2 we describe our galaxy model which is composed of halo, bulge, and disk components. The models of subhalos are also described in this section. In § 3 we present the results of our numerical simulations. In § 4 we analyze our results and present our prediction for the relation between the disk heating by subhalos and an observed thin or thick disk. Finally, in § 5 we present our conclusions.

2. Models

2.1. *The Galaxy Model*

Our galaxy model is composed of three components: a disk, a bulge, and a dark halo. To investigate the self-gravitating response of the disk component to orbiting subhalos, we model the disk by a self-consistent N-body realization of stars under the influence of an external force provided by the rigid bulge and halo components. The methods of Hernquist (1993) are utilized to set up the disk consisting of the distribution of N-body particles. A detailed description of the technique can be found in Hernquist's paper.

The density distribution of the disk is initially axisymmetric, $\rho_d(R,z)$, using the cylindrical coordinates (R,z), while the bulge and halo are spherically symmetric, $\rho_b(r)$ and $\rho_h(r)$, respectively, using the galactocentric distance r. These density distributions are given by

$$\rho_d(R,z) = \frac{M_d}{4\pi R_d^2 z_d} \exp(-R/R_d) \mathrm{sech}^2(z/z_d) \ , \tag{1}$$

$$\rho_b(r) = \frac{M_b}{2\pi} \frac{a_b}{r(a_b+r)^3} \ , \tag{2}$$

$$\rho_h(r) = \frac{M_h}{2\pi^{3/2}} \frac{\alpha_h}{r_c} \frac{\exp(-r^2/r_c^2)}{r^2+\gamma^2} \ , \tag{3}$$

where M_d, M_b and M_h correspond to the masses of the disk, the bulge and the halo, respectively. The disk parameters R_d and z_d denote the radial scale length and vertical scale height, respectively. The parameter a_b denotes the scale length of the bulge, while γ and r_c are the core and cut-off radii for the halo and α_h is a normalization constant. We choose these parameters so that the model approximately matches the observed characteristics of the Galaxy, and the values of the parameters are listed in Tabel 1. It is worth remarking that we consider an observed thin scale height for the disk, namely $z_d = 245$ pc, in contrast to the models by Font et al. (2001) and Velázquez & White (1999) adopting $z_d = 700$ pc. In order to prevent the disk from gravitational instability, we adopt a stable disk by setting Toomre's Q parameter at the solar radius $R_\odot = 8.5$ kpc as $Q_\odot = 1.5$. The rotation curve of our galaxy model is shown in Figure 1. The rotation speed at the solar radius is $V_c(R_\odot) \approx 240$ km s^{-1}.

2.2. *Subhalo Models*

We construct a set of subhalo models in our numerical simulations, designated as model A to U as tabulated in Table 2, to investigate how different physical properties of subhalos affect the disk heating process. Each model assumption is explained as follows.

2.2.1. *Mass function, spatial distribution and velocity anisotropy*

We consider a mass spectrum for the realization of each subhalo with a mass $M_{\rm sub}$. According to the results of cosmological N-body simulations by Moore et al. (1999), Klypin et al. (1999), and Ghigna et al. (2000), this mass function can be fitted to a power law with an index of about -2. We thus adopt the form,

$$N(M_{\rm sub}) dM_{\rm sub} \propto M_{\rm sub}^{-2} dM_{\rm sub} \ . \tag{4}$$

For the convenience of numerical analysis, we set the higher and lower mass limits for this mass function designated as $M_{\rm high}$ and $M_{\rm low}$, respectively, and examine the role of individual subhalo masses in the disk heating. The normalization of equation (4) is given by the total mass of the subhalo system, which is about one-tenth of the mass of a host halo according to Klypin et al. (1999) and Ghigna et al. (2000). We thus set $0.1M_h$ as the total mass of the subhalo system.

Recent high-resolution N-body simulations have shown that the spatial distribution of subhalos in a host halo is less concentrated than the host's density profile (Gao et al. 2004), which is often represented by the so-called NFW profile (Navarro, Frenk, & White 1997). However, in even most recent simulations the mass and force resolutions are yet insufficient, so the true spatial distribution of subhalos is unclear. In this paper, instead of trying to set a realistic spatial distribution (which is yet unknown), we adopt a tractable model for it and attempt to extract the general results which do not depend on this particular setting. Thus, for the initial spatial distribution of subhalos in a host halo, we adopt the Hernquist model (Hernquist 1990), in which the number density $n(r)$ of subhalos at the galactocentric distance r is given as

$$n(r) \propto \frac{1}{r(a+r)^3} \ , \tag{5}$$

where a is the scale length in the spatial distribution. It is worth noting that the inner density distribution of this model is similar to that of the NFW profile. The change of the parameter a affects the incidence of subhalo-disk interaction, which is mostly effective at $r \lesssim 10$ kpc, since smaller a yields smaller pericenters and apocenters for the orbits of subhalos. This is highlighted in Figure 2, where the distributions of the pericenters and apocenters of subhalos are shown for Model F ($a = 87.5$ kpc) and Model G ($a = 280$ kpc), while having the same velocity distribution (see below). It follows that the number of subhalos orbiting interior to r 10 kpc is larger for Model F than for Model G, and the dependence of this number on the scale length a is also seen in other models.

For the initial velocity distribution of subhalos, we take the moments of the collisionless Boltzmann equation following a procedure described by Hernquist (1993). The velocity ellipsoid at each spatial location is calculated from the moment equations, and then the velocity components are randomly selected from the Gaussian distributions for the corresponding velocity ellipsoid.

We adopt two different models for the velocity anisotropy of the subhalo system, which is parameterized by $\beta \equiv 1 - 0.5(\sigma_\theta^2 + \sigma_\phi^2)/\sigma_r^2$, where σ_r, σ_θ, and σ_ϕ are the radial, zenithal, and azimuthal velocity dispersions, respectively. One is the isotropic model of $\beta = 0$, which acts as our standard model. The other is the radially anisotropic model characterized by $\beta = 0.5$. This anisotropic model is motivated by the results of cosmological N-body simulations (Diemand et al. 2004; Abadi et al. 2006), which show the increase of β with r, starting $\beta \sim 0$ at a halo center to $\beta \gtrsim 0.5$ in its outer parts. For the sake of simplicity, we assume β is constant along r in our model.

2.2.2. Effect of Baryon Condensation

In hierarchical galaxy formation models, stars are formed in the condensation of cooled baryon in a halo center, subsequently forming a disk component. This condensed baryon or disk pulls the surrounding dark matter particles inward, thereby increasing the central concentration of a dark halo (e.g., Gnedin et al. 2004). This effect of baryon condensation is also expected to modify the space and velocity distributions of subhalos, compared with those obtained by dissipationless N-body simulations (Gao et al. 2004).

We take into account this effect in our model by slowly increasing the total masses of the disk and bulge components over a period of 10 Gyr, after setting the initial distribution of subhalos in the presence of a (smooth) halo alone. When the total masses of the disk and bulge components reach the values listed in Table 1, the position and velocity of each subhalo are recorded for the use of the further calculations of disk heating. In this experiment, we treat a subhalo as a point mass and neglect the interaction between different subhalos.

This treatment of the baryon condensation effect is admittedly highly ideal and not self-consistent as we neglect the simultaneous modification for a smooth halo component[1]. However, the rate of the interactions between subhalos and a disk is somewhat increased by this gravitational effect of baryonic matter, thereby allowing us to carry out a statistically meaningful analysis on the properties of the disk heating. In fact, this effect of baryon condensation results in a few percent increase in the number of subhalos having pericenters smaller than ~ 10 kpc, which yields the enough amount of interaction events over the interval of numerical simulations.

2.2.3. Internal Density Distribution

We consider two different models for the internal density distribution of a subhalo: point-mass and extended-mass models. In the former models, since point-mass subhalos survive eternally in our simulations, it is postulated that subhalos are supplied through their continuous accretion into a host halo from outside even if some of them disappear due to tidal destruction. In the latter models affected by tides, we assume a King-model profile characterized by a concentration parameter $c_{\rm King} = \log_{10}(R_t/R_c)$, where R_t and R_c denote tidal and core radii, respectively. For these latter models, the tidal effects of the disk (as well as the bulge and halo) on subhalos are explicitly taken into account. While the adoption of a King-model profile is admittedly ideal, recent cosmological simulations by Kazantzidis et al. (2004) imply that the internal density distributions of subhalos may be described reasonably well by a more-centrally concentrated universal profile or the NFW profile with some tidal outer limit. We therefore adjust our King models to match the NFW profile in the following manner. Firstly, based on the method outlined in NFW, we determine a set of model parameters in the NFW profile (see Appendix 1 for details). Secondly, we estimate a parameter $c_{\rm King}$, whereby the half-mass radius of the King model is equal to that of the NFW model. Finally, we obtain a tidal radius R_t as a limiting radius of the tidal effect of a host galaxy at the initial position of a subhalo. Thus, R_t is derived from the relation

$$\frac{M_{\rm tot}(<r)}{r^3} = \frac{M_{\rm sub}}{R_t^3}, \tag{6}$$

where $M_{\rm tot}(<r)$ is the total mass of a host galaxy interior to r and $M_{\rm sub}(<R_t)$ is the mass of a subhalo. For this estimation of R_t, we assume a spherically symmetric potential

[1] Our adoption of an isothermal-like profile for a smooth halo (equation 3), in comparison with an NFW-like profile derived from N-body simulations, suggests the consideration of baryon condensation for the halo setting.

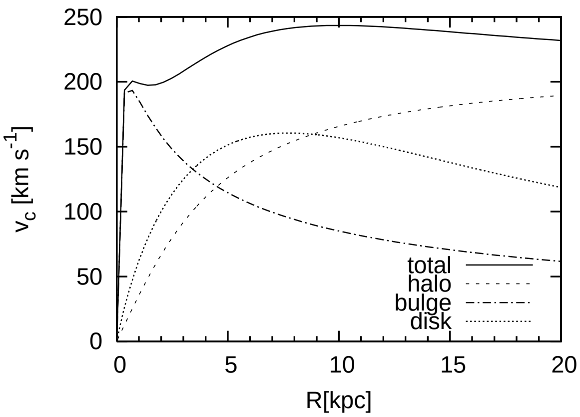

Fig. 1. Rotation curve for our disk galaxy model.

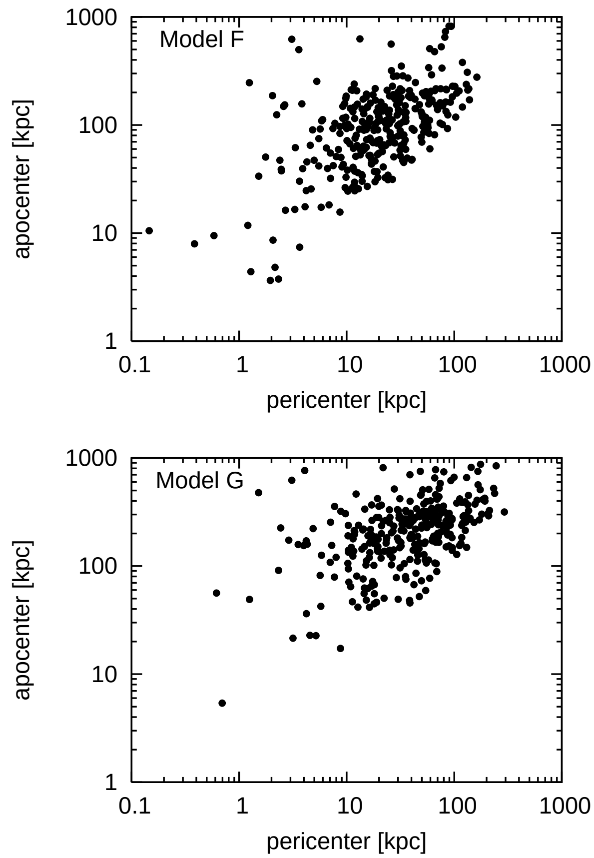

Fig. 2. Distributions of the pericenter and the apocenter of the subhalos in model F (left panel) and model G (right panel).

for a host galaxy, where the disk is made spherical with a mass distribution $M_d(r) = M_d[1-(1+r/R_d)\exp(-r/R_d)]$. We also take into account the effects of baryon condensation for getting the initial position of a subhalo.

The parameters for point-mass models and extended-mass models that we calculate are summarized in Table 2.

2.3. Method for Numerical Simulation

For the point-mass models we use a tree algorithm with a tolerance parameter of $\theta_{\rm tor} = 0.7$ (Barnes & Hut 1986; Hernquist 1987). For the extended-mass models we use GRAPE5 systems at the National Astronomical Observatory of Japan. The time integration is made with the leapfrog method and a fixed time step of 0.41 Myr. The softening length for N-body particles is $\epsilon = 70$ pc. We use $N_d = 46000$ particles for the disk and the number of the subhalo particles is listed in Table 2. Since the mass of the subhalo is negligibly small as compared with that of the host galaxy, we neglect the forces between the subhalos in the point-mass models. In contrast, for the extended-mass models, we fully take into account the gravitational interaction between the subhalos for the convenience of numerical calculations using GRAPE5. We have followed the evolution up to 4.9 Gyr.

3. Results

Based on the numerical simulations of the models defined in the previous section, we examine the effects of subhalos on the disk structure and dynamics, especially to elucidate the dependence of several different properties of subhalos: their internal density distribution, mass function, and spatial and velocity distributions.

In Figure 3 we show the edge-on view of the disk for model F at the beginning ($t = 0$) and the end ($t = 4.9$ Gyr) of the simulation. The disk has been thickened and tilted by the gravitational interaction with orbiting subhalos. To estimate the change of the disk kinematics and thickness at specific locations, we consider the tilt of the disk and use the axes aligned with the principal axes of the disk inertia tensor. The heating and thickening of the disk can be described by the changes of the velocity dispersions ($\Delta\sigma_R$, $\Delta\sigma_z$) and by the increase of the scale height, Δz_d. To calculate these quantities, the disk is stratified in concentric cylindrical annuli with a width of $\delta R = 700$ pc and the particle properties are averaged in each annulus. The scale height in each annulus R of the disk, z_d, is defined by the mean square of the z-coordinates, i.e., $z_d(R) \equiv < z^2 >^{1/2}$. We note that at the beginning of the calculations, z_d is a constant of 245 pc as given in equation (1).

In addition to the dynamical effect of subhalos, the simulated disk is subject to internal heating due to two-body relaxation among the disk particles; this numerical heating always takes place in numerical simulations with a modest number of particles. We evaluate the effect of internal heating by evolving the disk in isolation, i.e., in the absence of subhalos. This effect is typically characterized as $\Delta z_d = 0.23$ kpc, $\Delta\sigma_R = 7.2$ km s^{-1}, and $\Delta\sigma_z = 5.7$ km s^{-1} at the solar radius after 4.9 Gyr. In the followings, the notation Δz_d means the difference of a scale height between $t = 4.9$ Gyr and $t = 0$, and $\Delta\sigma_R$ and $\Delta\sigma_z$ also mean the change of the velocity dispersions after 4.9 Gyr.

3.1. Global Properties of the Disk Evolution

In Figure 4 we show the kinematical properties of the disk for model A, F and G, including the impact of internal heating in our calculations. It is evident from this figure that thickening of the disk does not occur uniformly at all radii; given the complexity of the final disk structure, we found it convenient to sample the kinematics at $R = R_\odot$, $3R_d$, and $4R_d$, which is sufficient to provide us with a global view of the heating and thickening. The growth of the disk thickness in model A is $\Delta z_d \sim 0.57$ kpc, 0.61 kpc and 0.67 kpc at $R = R_\odot$, $3R_d$, and $4R_d$, respectively, those values in model F are 1.19 kpc, 1.37 kpc and 1.60 kpc, and those values in model G are 0.28 kpc, 0.31 kpc, and 0.39 kpc. The increase in the radial and vertical velocity dispersions after 4.9 Gyr in model A is given as $(\Delta\sigma_R, \Delta\sigma_z) = (18.8, 15.4)$, $(17.4, 13.8)$, and $(16.6, 11.9)$ km s^{-1} at $R = R_\odot$, $3R_d$, and $4R_d$, respectively, those values in model F are (32.2,26.1), (30.1,23.9), and (25.4,22.8) km s^{-1}, and those values in model G are (9.9,8.2), (10.5,7.5) and (13.5,8.2) km s^{-1}.

In these experiments, the main difference between model A and model F resides in individual masses of subhalos parameterized by $M_{\rm high}$ and $M_{\rm low}$ (see Table 2): for model A all subhalos have 10^8 $M_\odot$ as $M_{\rm high} = M_{\rm low} = 10^8$ $M_\odot$, whereas for model F the presence of more massive subhalos than 10^8 $M_\odot$ is allowed as $M_{\rm high} = 10^9$ $M_\odot$. Therefore the comparison between the results of these two models highlights the effect of individual masses of subhalos on the disk heating, where we note that the slight difference of the parameter a between the models by a factor 1.25 yields essentially no difference in the results. It is clear that the presence of a few, but massive subhalos (model F) is more effective for the disk heating than the case of many but less massive ones (model A), as already pointed out by Ardi et al. (2003). This suggests that the disk heating process is more sensitively enhanced than being proportional to individual subhalo masses; massive subhalos are more important for the disk heating. Also, in comparison with model F, model G with the same values for $M_{\rm high}$ and $M_{\rm low}$ yields a weak effect on the disk. The main difference between these two models is the spatial distribution of subhalos parameterized by a ($a = 87.5$ kpc and 280 kpc for model F and G, respectively), which affects the pericenter distributions of subhalos especially at $r \lesssim 10$ kpc (see Figure 2). Therefore, we find that the number of subhalos which cross the disk is also important in quantifying the disk heating.

Figure 5 shows the growth of disk velocity dispersions in the radial and vertical directions at $R = R_\odot$ for model F (the point-mass model), K and L (the extended-mass model). This figure shows that the disk velocity dispersion for model F continues to grow throughout the simulations, whereas for model K and L the growth of the velocity dispersion almost stops at $t \sim 1$ Gyr. It is worth noting that in these latter models subhalos can lose their mass at the interaction with the disk, unlike the former point-mass models in which subhalo masses remain the same. Thus, for the extended-mass models the effect of subhalos

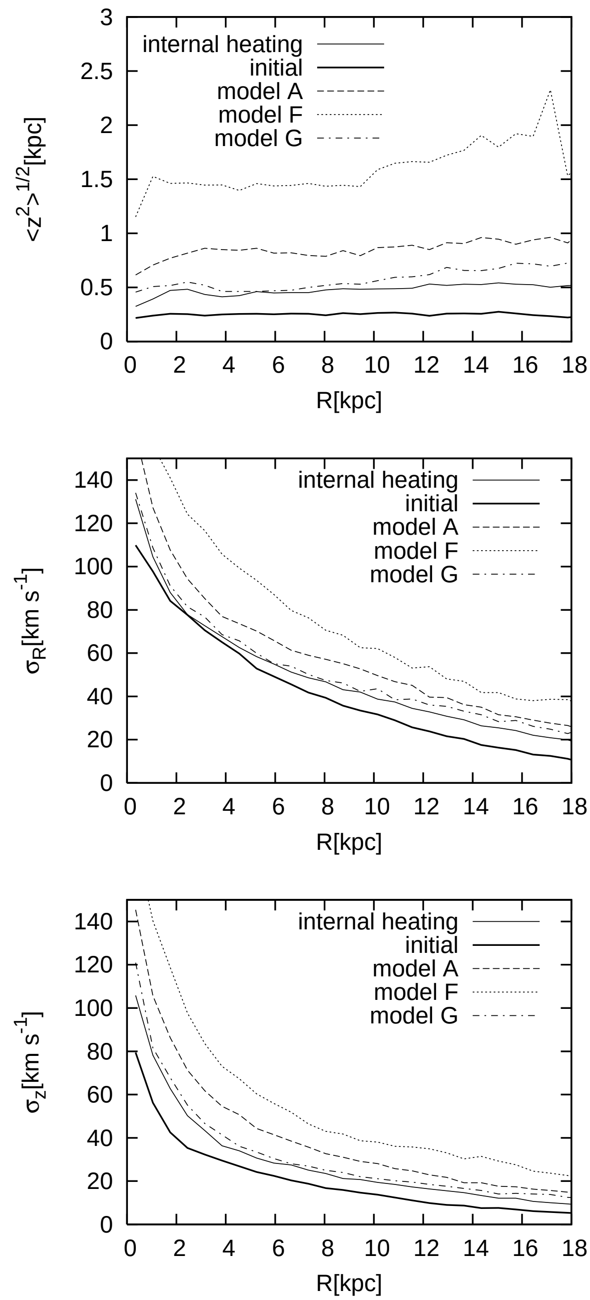

Fig. 4. The kinematical properties of the disk after 4.9 Gyr for different subhalo models. Thick solid lines show the initial setting and thin solid lines show the effects of internal heating in the absence of subhalos. Dashed, dotted, and dash-dotted lines show model A, F, and G, respectively.

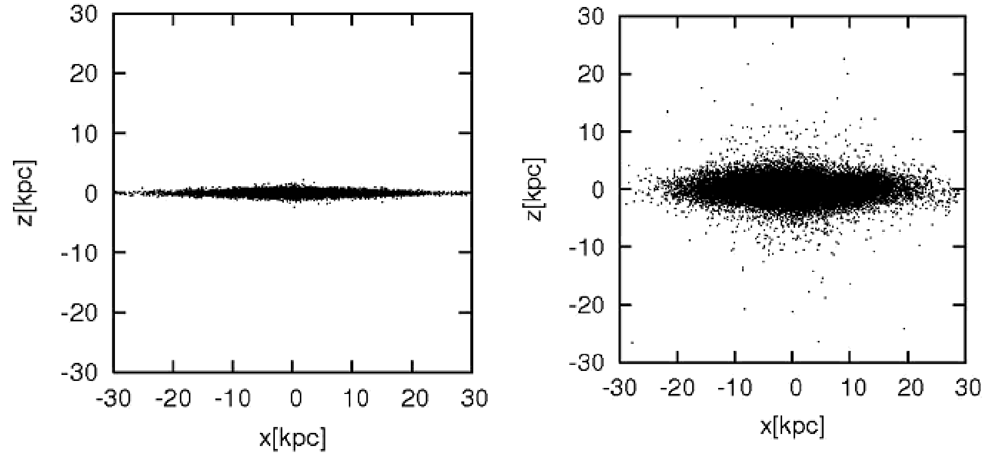

Fig. 3. Growth of the disk thickness for model F. The left and right panels show the egde-on view of the disk at the beginning ($t = 0$) and the end ($t = 4.9$ Gyr) of the simulation, respectively.

on the disk is temporal; subhalos appear to lose almost all of their mass at the first interaction with the disk, so that their role in the disk heating is effective only at the first interaction with the disk.

3.2. *Disk Thickness vs. Subhalo Masses*

In this section we investigate in more detail the effect of orbiting subhalos on the growth of the disk thickness. As discussed above, the change of the disk scale height, z_d, depends on R, in such a manner that Δz_d is somewhat larger at larger R. To quantify this disk thickening as a function of accreted subhalo masses, we utilize the disk scale height at the outer edge of the disk, $R = R_{\rm out}$, where the stellar light distribution is expected to diminish steeply with R. This truncation of a stellar disk has actually been observed, where the stellar light declines more steeply than an exponential profile for a main disk and drops to low values beyond the so-called truncation radius (van der Kruit & Searle 1981a, b, 1982; Kregel et al. 2002). This usually occurs at a radius of $3-5$ disk scale length (Kregel et al. 2002), so in our work we adopt $R_{\rm out} = 3R_d$ as a characteristic outer edge of the disk, at which the change of the disk scale height is evaluated. Also, to analyze the relation between the change of the disk thickness and the orbits of the accreted subhalos, we estimate the number of times which each subhalo crosses the disk region at $R \leq 3R_d$ in the course of its orbital motion.

We have carried out the simulations for several different models of point-mass subhalos with $\beta = 0$. Figure 6 shows the relation between the growth of the disk scale height at $R = 3R_d$ (i.e. $\Delta z_d/R_d$) and the combination of each mass of a subhalo $M_{{\rm sub},i}$ and the number of times which it crosses the disk at $R \leq 3R_d$ in the course of its orbital motion, denoted as N_i [i.e. $\sum_i N_i(M_{{\rm sub},i}/M_d)$ for the left panel and $\sum_i N_i(M_{{\rm sub},i}/M_d)^2$ for the right panel]. Here the abscissa for the left panel is proportional to the total accreted mass of subhalos, whereas that for the right panel is proportional to the sum of the squared masses

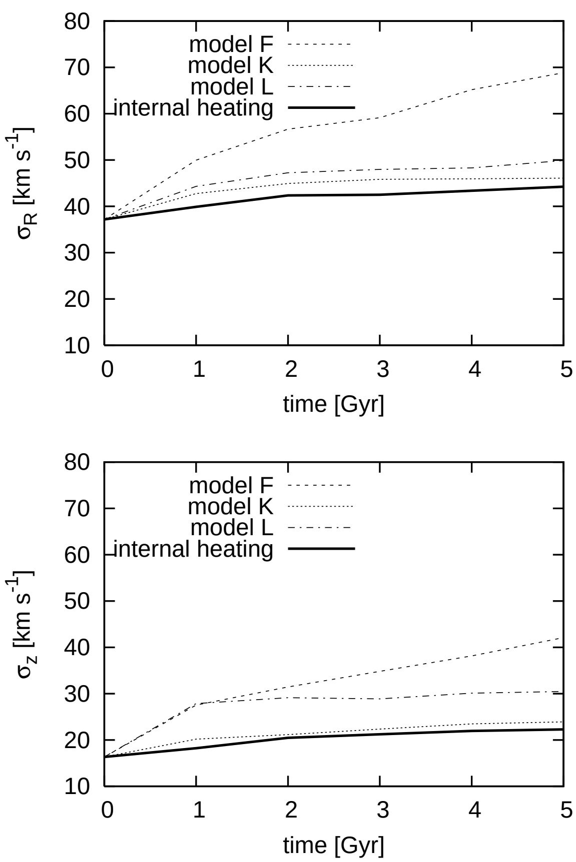

Fig. 5. Growth of the disk velocity dispersion in the radial and vertical directions at $R = R_\odot$ for model F (dashed lines), K (dotted lines), and L (dash-dotted lines). In model F subhalos are represented by point masses, whereas in model K and L they have a King-model profile. Thick solid lines show the effect of internal heating in the absence of subhalos.

of subhalos. As is evident, while the left panel shows no correlation between the abscissa and ordinate axes, the right panel shows a significantly tight correlation, thereby indicating that the growth of the disk thickness is proportional to the sum of the squared masses of subhalos; if so, the disk thickening is more enhanced for more massive individual subhalos as already shown in the previous subsection. We thus investigate this relation for different subhalo models as shown in Figure 7. In the left panel we consider the extended-mass models with $\beta=0$ (filled squares) in comparison with the point-mass models with $\beta=0$ (open circles). We note here that in the extended-mass models subhalos lose almost all of their mass at the first interaction with the disk, so we adopt $N_i=1$ for such a case. The right panel shows the case of an anisotropic velocity distribution with $\beta=0.5$ for the point-mass models (filled triangles) and with $\beta=0$ for the point-mass models (open circles). As is evident from these panels, several different models yield an almost universal relation between $\Delta z_d/R_d$ at $R=3R_d$ and $\sum_i N_i(M_{\mathrm{sub},i}/M_d)^2$ at $R\leq 3R_d$.

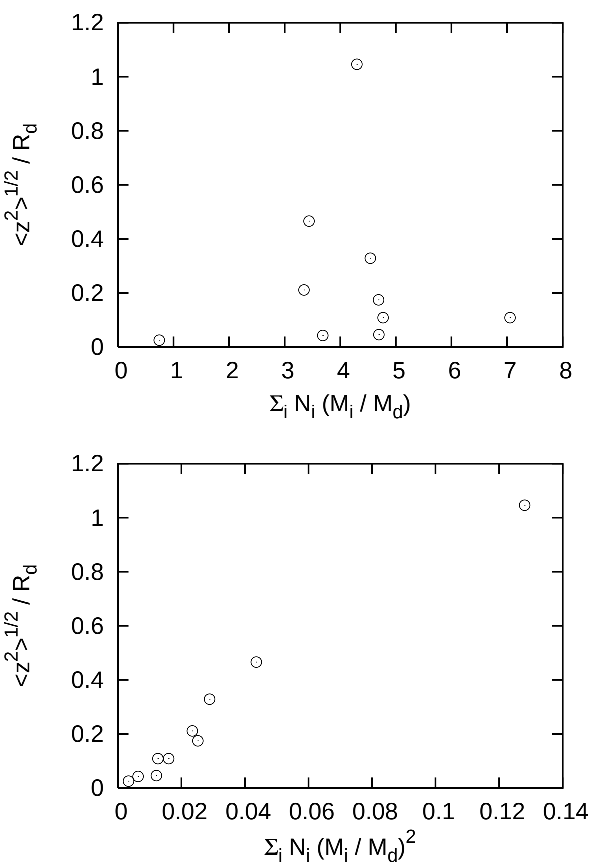

Fig. 6. Relation between the growth of the disk scale height at $R=3R_d$ and the combination of each mass of a subhalo $M_{\mathrm{sub},i}$ and the number of times which it crosses the disk at $R\leq 3R_d$, denoted as N_i, for the point-mass subhalo models with $\beta=0$ (model A to J listed in Table 2). The abscissas in the left and right panels show $\sum_i N_i(M_{\mathrm{sub},i}/M_d)$ and $\sum_i N_i(M_{\mathrm{sub},i}/M_d)^2$, respectively. Notice that the effect of internal heating has been subtracted in these plots.

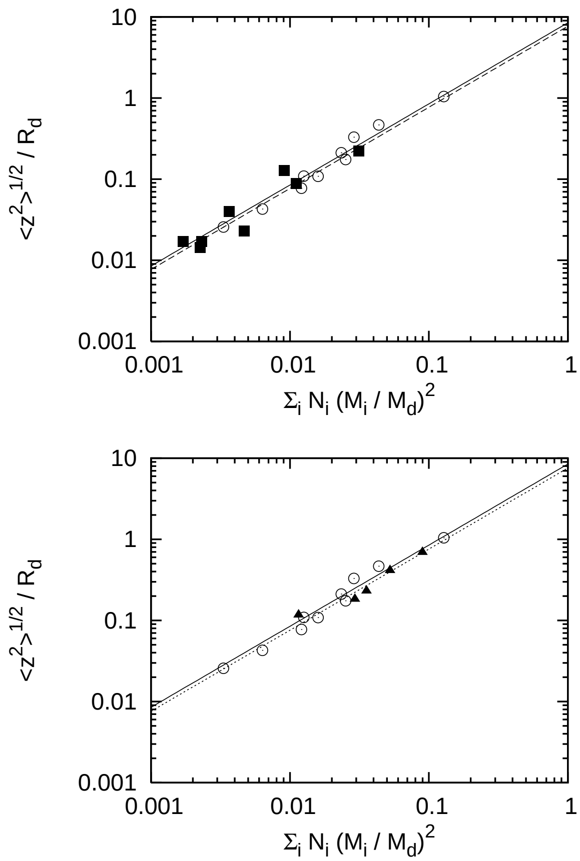

Fig. 7. The same as Figure 6 but for several different subhalo models plotted in logarithmic scales. The left panel shows the extended-mass models with $\beta=0$ (filled squares) in comparison with the point-mass models with $\beta=0$ (open circles), whereas the right panel shows the case of an anisotropic velocity distribution with $\beta=0.5$ for the point-mass models (filled triangles) and point-mass models with $\beta=0$ (open circles). The solid lines show the fitting to the relations for the point-mass models with $\beta=0$ by the least-squares method, dashed lines for the extended-mass models with $\beta=0$, and dotted lines for the point-mass models with $\beta=0.5$.

4. Discussion

4.1. Dependence of the Disk Heating on Subhalo Masses

From the results of § 3.2, we find that the disk thickness is increasing with the accretion of subhalos into a disk. Our numerical experiments suggest the following universal relation,

$$\frac{\Delta z_d}{R_d}=\alpha\sum_i N_i\left(\frac{M_{\mathrm{sub},i}}{M_d}\right)^2 \ , \tag{7}$$

where α is a constant of $\simeq 8$, R_d is the disk scale length, z_d is the disk scale height at $R=3R_d$, and N_i is the number of times that subhalos with an individual mass of $M_{\mathrm{sub},i}$ cross a disk at $R\leq 3R_d$ (noting that $N_i=1$ for the extended-mass models as subhalos lose their mass at their first interaction with the disk). In this expression, a subscript i denotes an individual subhalo given at $t=0$

in our simulation. An alternative, more useful expression based on equation (7) is derived as follows. Supposing that the disk has experienced the accretion of subhalos having an individual mass of $M_{\rm sub,j}$ with $j = 1, ..., N$ at $R \leq 3R_d$, where the repeated accretion of a subhalo in the course of its orbital motion is regarded as a separate accretion event with a mass $M_{\rm sub,j}$, and N denotes the total number of such events. Then, we obtain the relation,

$$\frac{\Delta z_d}{R_d} \simeq 8 \sum_{j=1}^{N} \left(\frac{M_{\rm sub,j}}{M_d} \right)^2 , \tag{8}$$

which holds a more useful form for any applications than equation (7). Notice that although this relation is derived from the simulations over the interval of 4.9 Gyr, this is applicable to longer time evolution by considering the total number of subhalos crossing a disk, N.

As equation (8) indicates, the increase of the disk thickness is proportional to the square of the masses of accreted subhalos. This mass dependency in the disk heating process can be understood if we consider the transfer of kinetic energy from the subhalos to the disk through dynamical friction. Here we present the summary of this derivation and more details are shown in Appendix 2.

Firstly, the vertical equilibrium between kinetic and gravitational energy allows us to relate the velocity dispersion σ_z and the scale height z_d of a disk. Assuming that a disk is an isothermal sheet, we obtain

$$\sigma_z^2 = 2\pi G \Sigma(R) z_d , \tag{9}$$

where $\Sigma(R)$ is a surface density of a disk at R (e.g. Spitzer 1942). Secondly, we consider the energy input into disk stars getting through subhalo-disk interaction: the energy loss of a subhalo is equal to the energy pumped into a disk. This energy loss $\Delta E_{\rm sub}$ is derived by the integral over an orbit of a subhalo,

$$\Delta E_{\rm sub} = \int F_{\rm drag} ds , \tag{10}$$

where $F_{\rm drag}$ corresponds to a dynamical friction. Using the Chandrasekhar formula for $F_{\rm drag}$, each subhalo with a mass $M_{\rm sub}$ is subject to a frictional force with $F_{\rm drag} \propto M_{\rm sub}^2$. Finally, combining equation (9) with (10), we obtain,

$$\Delta z_d \propto \Delta \sigma_z^2 \propto \Delta E_{\rm sub} \sim F_{\rm drag} \cdot z_d \propto M_{\rm sub}^2 . \tag{11}$$

Therefore, the dependence of Δz_d on $M_{\rm sub}$ as we have obtained in § 3 is understood in the framework of a dynamical friction between a subhalo and a disk.

4.2. *Comparison with an Observed Thin Disk*

Recent observations of external disk galaxies by Kregel et al. (2002) have suggested that the thickness of a (thin) disk is confined to some limiting value relative to a scale length of a disk, which is expressed as $z_d/R_d < 0.2$. Kregel et al. (2002) have also shown that the distribution of z_d/R_d tends to have an increasing dispersion with increasing maximum circular velocity V_c of a disk, in such a manner that larger V_c allows smaller z_d/R_d; conversely, a disk with smaller V_c is likely thicker.

An observed thin disk with $z_d/R_d < 0.2$ suggests that the accretion of subhalos has been rather insignificant since a disk with a current mass was formed. Using equation (8), this observed limit implies $(\sum_j M_{\rm sub,j}^2)^{1/2} < 0.15 M_d$. Thus, we find that an observed thin disk has not ever interacted with subhalos with the total mass of more than 15 % disk mass.

The dependence of z_d/R_d on V_c may be understood as follows. Let $\langle M_{\rm sub}^2 \rangle$ as the mean square of a subhalo mass, defined as $\langle M_{\rm sub}^2 \rangle = \sum_j^N M_{\rm sub,j}^2 / N$. Then, equation (8) can be written as

$$\frac{\Delta z_d}{R_d} \propto N \frac{\langle M_{\rm sub}^2 \rangle}{M_d^2} . \tag{12}$$

We suppose that N, the number of subhalos which cross a disk at $R \leq 3R_d$, is roughly proportional to the spherical volume with a radius $3R_d$ inside a dark halo, given the spatial distribution of subhalos. This reads $N \propto R_d^3$. Also suppose that the central disk surface density $\Sigma_0 = M_d/(2\pi R_d^2)$ is nearly the same for a disk galaxy, which may correspond to nearly the same central surface brightness for a bright disk (e.g., Freeman 1970). Then equation (12) is rewritten as,

$$\frac{\Delta z_d}{R_d} \propto \langle M_{\rm sub}^2 \rangle \cdot V_c^{-2} , \tag{13}$$

where V_c is a disk circular velocity derived from $V_c \propto GM_d/R_d$.

Thus, if the observed disk thickness is controlled by disk-subhalo interaction, i.e., $z_d \sim \Delta z_d$, and $\langle M_{\rm sub}^2 \rangle$ is roughly the same for each disk galaxy, then we find that the effect of subhalos on a disk with a smaller mass is more significant than a disk with a larger mass. This is in good agreement with the observation (Kregel et al. 2002) that a disk with smaller V_c is likely thicker.

4.3. *The Relation to the Origin of a Thick Disk*

In recent years, new datasets for the thick disk component of the Galaxy as well as for a thick disk of an external galaxy have been available, showing several important properties of a thick disk. Based on the third data release of the Sloan Digital Sky Survey (York et al. 2000), Allende Prieto et al. (2006) have found that the stars belonging to the thick disk have no vertical metallicity gradient. The rotational velocity for the same stars however shows a vertical gradient of ~ -16 km s^{-1} kpc^{-1} between 1 and 3 kpc from the Galactic plane. The observations of an external disk galaxy (Yoachim & Dalcanton 2006) have shown that the ratio of the total luminosity of a thick disk to that of a thin one is related to the circular velocity of a galaxy, in such a manner that the ratio tends to increase with decreasing circular velocity; a less massive galaxy has a brighter (and possibly more massive) thick disk relative to a thin one. These properties of a thick disk are expected to set important constraints on its origin.

Here, we consider a possibility that a thick disk has been formed by the dynamical effect of numerous dark subhalos on a pre-existing disk. This interaction effect may be rather weak at the current epoch as only a small fraction of subhalos would cross a disk (Font et al. 2001), but the effect at early times may have been more significant due to a smaller disk mass and larger accretion rate of subhalos onto a parent halo. If so, a pre-existing disk should have suffered from considerable heating at early times, which results in the formation of a thick disk; subsequent slow accumulation of baryonic gas in a plane may form a thin disk component.

To assess this possibility in light of the observed properties of a thick disk, we investigate the properties of the disk thickened by subhalos in our model. Figure 8 shows the distribution of the stars in model F at the end of the simulation ($t=4.9$ Gyr), differentiated by the initial ($t=0$) positions at either $z<245$ pc (left panel) or $z>245$ pc (right panel). As is evident, the disk stars are well mixed by the disk heating. This suggests that even if a pre-existing disk had a metallicity gradient, the disk heating by interactions with subhalos would have wiped out this gradient, leaving a thick disk in agreement with the observations. It is also suggested that this disk heating process prompts a vertical gradient in rotational velocity. This is explained as follows. A heated disk puffs up not only in the vertical but also in the radial direction, where the stars located at high $|z|$ have large radial velocity dispersion compared with those at low $|z|$ and thus have small rotational velocities on average due to the effect of asymmetric drift: given a gravitational force inward, the increase of radial pressure of stars reduces the effect of a centrifugal force. This vertical gradient in rotational velocity is actually obtained in our simulation models as shown in Figure 9. It is found that the gradient amounts to $-10\sim-30$ km s^{-1} kpc^{-1} between 1 and 3 kpc from the plane, in good agreement with the observations. This experiment suggests that the presence of a vertical gradient in rotational velocity of a thick disk may be an important clue to distinguishing the scenarios for the origin of a thick disk; models invoking monolithic disk collapse (Burkert, Truran & Hensler 1992) or chaotic merging event of building blocks (Brook et al. 2004) at early times of a galaxy may have difficulties in this regard.

More definite picture for the formation of a thick disk must await more elaborate modeling of a forming galaxy in the context of hierarchical clustering. In particular, each galaxy has a different merging history of subhalos and so different spatial and velocity distributions, which inevitably affects the interpretation for the observed properties of a thick disk, such as for its fraction as a function of a disk mass. Also, the observations show that almost all of disk galaxies have a distinct thick disk in addition to a thin component. This implies that the dynamical effects of subhalos on a disk were significant only before a specific epoch and the subsequent formation of a thin disk has been unaffected by subhalos, although it is yet unclear if it is applicable to all galaxy-sized halos having different merging histories. Therefore, to assess the scenario, more detailed numerical studies are required, taking into account the growth of both a dark halo and disk simultaneously.

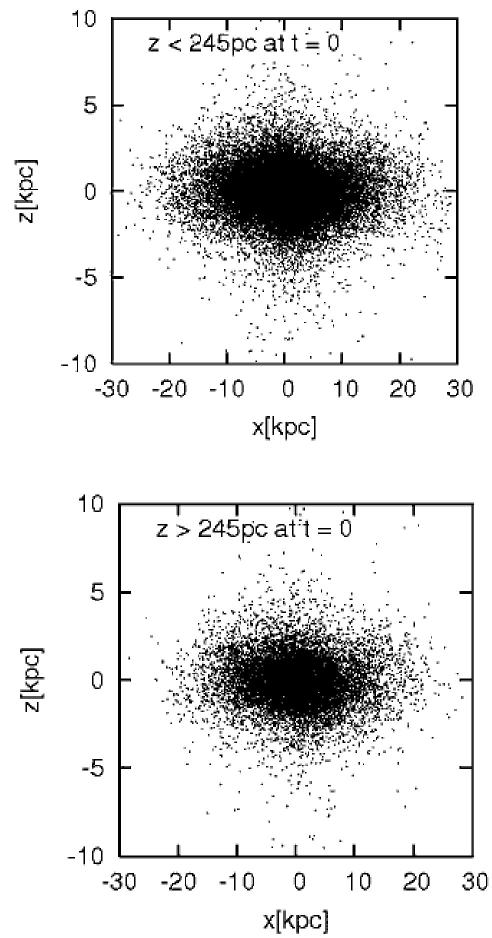

Fig. 8. Distribution of stars in model F at the end of the simulation ($t=4.9$ Gyr), differentiated by their initial ($t=0$) positions at $z<245$ pc (left panel) and $z>245$ pc (right panel).

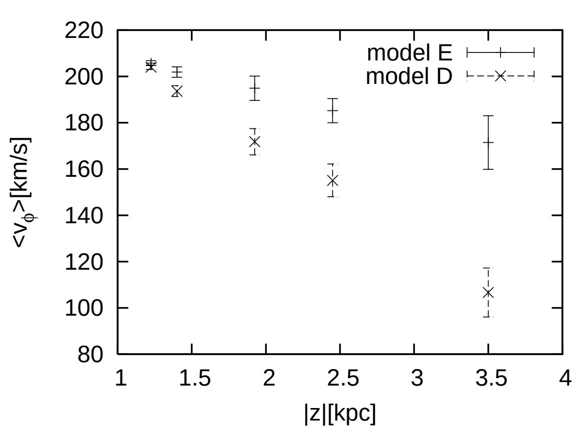

Fig. 9. Mean azimuthal velocity of the stars located at annulus $R=R_{\odot}\pm1.05$ kpc as a function of the distance away from the plane, for model D and E. Note that both models show similar vertical scale height $z_d\approx1$ kpc at the end of the simulations ($t=4.9$ Gyr).

5. Conclusions

We summarize our conclusions as follows:

- The dynamical effects of subhalos on a disk are represented by the relation between the change of the disk scale height Δz_d (measured at the disk edge $R = 3R_d$) and individual masses of subhalos $M_{\rm sub}$, i.e., $\Delta z_d/R_d \simeq 8\sum_{j=1}^{N}(M_{{\rm sub},j}/M_d)^2$, where R_d is a disk scale length, M_d is a disk mass, and N is the total number of accretion events of subhalos inside a disk region ($\leq 3R_d$).
- If subhalos with the total mass of more than 15 % disk mass interact with a disk, then the disk thickness is made larger than the observed range.
- A less massive disk with smaller circular velocity V_c is found to be more affected by subhalos than a disk with larger V_c, which is in agreement with the observed properties of a thin disk.
- Stars in a significantly thickened disk by subhalos appear to be well mixed and show a vertical gradient in their rotation velocity, being similar to the observed properties of the thick disk in the Galaxy.

We note that the relation (8) we have obtained here is universal and thus useful for the applications to any relevant issues, including the dynamics of an evolving stellar disk at the center of a growing dark halo. Such detailed studies of a galactic disk in comparison with recently increasing datasets of a remote disk galaxy will be of great importance and is left to future work.

The numerical computations reported here were carried out on GRAPE systems (project ID: g05b05) kindly made available by the Astronomical Data Analysis Center (ADAC) at the National Astronomical Observatory of Japan (NAOJ). This work has been supported in part by a Grant-in-Aid for Scientific Research (15540241, 17540210) from the Japanese Ministry of Education, Culture, Sports, Science and Technology.

References

Abadi, M., Navarro, J. F., & Steinmetz, M 2006, MNRAS, 365, 747
Allende Prieto, C., Beers, T. C., Wilhelm, R., Newberg, H., J., Rockosi, C. M., Yanny, B., & Lee, Y. S., 2006, 636, 804
Ardi, E., Tsuchiya, T., & Burkert, A. 2003, ApJ, 596, 204
Barnes, J. E., Hut, P. 1986, Nature, 324, 446
Brook, C. B., Kawata, D., Gibson, B. K., & Freeman, K. C. ApJ, 612, 894
Burkert, A., Truran, J. W., & Hensler, G. 1992, ApJ, 391, 651
Diemand, J., Moore, B., & Stadel, J. 2004, MNRAS, 352, 535
Font, A. S., Navarro, J. F., Stadel, J, & Quinn, T. 2001, ApJ, 563. L1
Freeman, K. C. 1970, ApJ, 160, 811
Gao, L., White, S. D. M., Jenkins, A., Stoehr, F., & Springel, V. 2004, MNRAS, 355, 819
Ghigna, S., Moore, B., Governato, F., Lake, G., Quinn, T., & Stadel, J. 2000, ApJ, 544, 616
Gnedin, O. Y., Kravtsov, A. V., Klypin, A. A., & Nagai, D. 2004, ApJ, 616, 16
Hernquist, L. 1987, ApJS, 64, 715
Hernquist, L. 1990, ApJ, 356, 359
Hernquist, L. 1993, ApJS, 64, 715
Kazantzidis, S., Mayer, L., Mastropietro, C., Diemand, J., Stadel, J., &, Moore, B. 2004, ApJ, 608, 663
Kregel, M., van der Kruit, P. C., & de Grijs, R. 2002, MNRAS, 334, 646
Klypin, A., Kravtsov, A. V., Valenzuela, O., & Prada, F. 1999, ApJ, 522, 82
Lacey, C. G., & Cole, S. M. 1993, MNRAS, 262, 626
Moore, B., Ghigna, S., Governato, F., Lake, G., Quinn, T., Stadel, J., & Tozzi, P. 1999, ApJ, 524, L19
Navarro, J. F., Frenk, C. S., & White, S. D. M. 1997, ApJ, 490, 493 (NFW)
Spitzer, L. 1942, ApJ, 95, 329
Summers, F. J., Davis, M., & Evrard, A. E. 1995, ApJ, 454, 1
Tóth, G., & Ostriker, J. P. 1992, ApJ, 389, 5
van der Kruit, P. C., & Searle, L. 1981a, A&A, 95, 105
van der Kruit, P. C., & Searle, L. 1981b, A&A, 95, 116
van der Kruit, P. C., & Searle, L. 1982, A&A, 110, 61
Velázquez, H., & White, S. D. M. 1999, MNRAS, 304, 254
Yoachim, P., & Dalcanton, J. J. 2006, ApJ, 131, 226
York, D. G. et al. 2000, ApJ, 120, 1597

Appendix 1. NFW profile

The NFW density profile is given by

$$\rho = \rho_{\rm crit}\frac{\delta_0}{(r/r_s)(1+r/r_s)^2}\ , \tag{A1}$$

where $\rho_{\rm cirt}$ is the critical density of the Universe, r_s is a scale radius, and δ_0 is a characteristic density contrast. Following NFW, we define the limiting radius of a virialized halo, r_{200}, to be the radius within which the mean mass density is $200\rho_{\rm crit}$. Also, the concentration parameter of a halo is defined as $c = r_{200}/r_s$, with which δ_0 is given as

$$\delta_0 = \frac{200}{3}\frac{c^3}{[\ln(1+c) - c/(1+c)]}\ . \tag{A2}$$

To put the NFW density profile in a cosmological context, we need to calculate the concentration factor c, which is related to δ_0 via equation (A2). The appropriate value of c depends on halo formation history and on cosmology. NFW proposed a simple model for c based on halo formation time. The formation redshift $z_{\rm coll}$ of a halo identified at $z = 0$ with mass M is defined as the redshift by which half of its mass is in progenitors with mass exceeding fM, where f is a constant. With this definition, $z_{\rm coll}$ can be computed by simply using the Press-Schechter formalism (e.g. Lacey & Cole 1993),

$$\mathrm{erfc}\left\{\frac{\delta_{\rm c}(z_{\rm coll}) - \delta_{\rm c}^0}{\sqrt{2[\Delta_0^2(fM) - \Delta_0^2(M)]}}\right\} = \frac{1}{2}\ , \tag{A3}$$

where $\Delta_0^2(M)$ is the linear variance of the power spectrum at $z = 0$ smoothed with a top-hat filter of mass M, $\delta_{\rm c}(z)$ is the density threshold for spherical collapse by redshift z, and $\delta_{\rm c}^0 = \delta_{\rm c}(0)$. NFW found that the characteristic overdensity of a halo at $z = 0$ is related to its formation redshift $z_{\rm coll}$ by

$$\delta_0(M,f) = C(f)\Omega_0[1+z_{\rm coll}(M,f)]^2 \ , \tag{A4}$$

where the normalization $C(f)$ depends on f and Ω_0 is the current density parameter of the Universe. We will take $f = 0.01$ as suggested by the N-body results of NFW. In this case $C(f) \approx 3\times 10^3$. Thus, for a halo of given mass at $z = 0$, one can obtain the concentration factor c from equations (A2)-(A4). In practice, we first solve $z_{\rm coll}$ from equation (A3) and insert the value of $z_{\rm coll}$ into equation (A4) to get δ_0. We then use this value of δ_0 in equation (A2) to solve for c.

In this experiment, we adopt a standard set of cosmological parameters as $\Omega_0 = 0.3$, $\Lambda = 0.7$, $h = 0.7$, and $\sigma_8 = 1.3$, where Λ is a cosmological constant, h is a normalized Hubble constant of $h \equiv H_0/100$ km s^{-1} Mpc^{-1}, and σ_8 parameterizes density fluctuations at 8 h^{-1} Mpc.

Appendix 2. Derivation of equation (8)

We show here the derivation of equation (8) based on the following dimensional analysis.

Firstly, we derive the relation between the vertical velocity dispersion σ_z of disk stars and the scale height z_d of a self-gravitating axisymmetric disk in cylindrical coordinates (R,z). For the limit of a thin disk where z-derivatives dominate over R-derivatives, an equation for vertical equilibrium and a Poisson equation read, respectively,

$$\frac{1}{\rho_d}\frac{\partial(\rho_d\sigma_z^2)}{\partial z} + \frac{\partial\Phi}{\partial z} \simeq 0 \ , \quad \frac{\partial^2\Phi}{\partial z^2} \simeq 4\pi G\rho \ , \tag{A5}$$

where ρ_d is a mass density of a disk and Φ is a gravitational potential. Integrating the second equation over all z gives the surface mass density $\Sigma(R)$ vs. Φ, i.e., $2\pi G\Sigma(R) \simeq \partial\Phi/\partial z$. Then, inserting this into the first equation, and assuming $\rho_d \propto \exp(-z/z_d)$ and σ_z is constant, we obtain $z_d \simeq \sigma_z^2/2\pi G\Sigma(R)$. This equation suggests that the change of the disk thickness is related to the change of the velocity dispersion, i.e.,

$$\Delta z_d \simeq \frac{\Delta\sigma_z^2}{2\pi G\Sigma(R)} \ . \tag{A6}$$

Secondly, the change of the velocity dispersion $\Delta\sigma_z^2$ is related to the energy input into disk stars getting through subhalo-disk interaction: the energy loss of a subhalo is equal to the energy pumped into a disk. Denoting this energy loss as $\Delta E_{\rm sub}$ per a subhalo, the resultant $\Delta\sigma_z^2$ for a disk with a total mass M_d reads,

$$\Delta\sigma_z^2 = \frac{2\Delta E_{\rm sub}}{M_d} \ . \tag{A7}$$

We note that $\Delta E_{\rm sub}$ is derived by the integral over an orbit of a subhalo,

$$\Delta E_{\rm sub} = \int F_{\rm drag} ds \sim F_{\rm drag} z_d \ , \tag{A8}$$

where $F_{\rm drag}$ corresponds to a dynamical friction. Using the Chandrasekhar formula for $F_{\rm drag}$, each subhalo with a mass $M_{\rm sub}$ is subject to a frictional force with

$$F_{\rm drag} = \frac{4\pi G^2 M_{\rm sub}^2 \rho_d \ln\Lambda}{v_{\rm sub}^2}\left[{\rm erf}(X) - \frac{2X}{\sqrt{\pi}}e^{-X^2}\right] \ , \tag{A9}$$

where $\ln\Lambda$ is the Coulomb logarithm, $X \equiv v_{\rm sub}/\sqrt{2}\sigma$ with σ being the disk velocity dispersion, and $v_{\rm sub}$ is the subhalo's velocity. For $v_{\rm sub}$, we suppose that it is represented by a virial velocity of a smooth dark halo with a mass M_H and a radius r_H, giving $v_{\rm sub}^2 \sim GM_H/r_H$. Furthermore, if M_d and R_d for a disk is some fraction of M_H and r_H, given as $M_d = f_1 M_H$ and $R_d = f_2 r_H$, where typically $f_1 \sim f_2 \sim O(10^{-1})$, we obtain $v_{\rm sub}^2 \sim GM_d/R_d$. For ρ_d, we set $\rho_d \sim M_d/R_d^2 z_d$.

Finally, using the above equations, the change of the disk thickness induced by N accretion events of subhalos is estimated by,

$$\Delta z_d \propto \frac{N\Delta\sigma_z^2}{G\Sigma} \propto \frac{NG^2 z_d M_{\rm sub}^2 \rho_d / v_{\rm sub}^2}{G\Sigma M_d} \propto \frac{NM_{\rm sub}^2}{\Sigma M_d R_d} \ . \tag{A10}$$

Thus, we obtain

$$\frac{\Delta z_d}{R_d} \propto N\frac{M_{\rm sub}^2}{M_d^2} \ , \tag{A11}$$

which is consistent with equation (8).

Table 1. Galactic parameters

	Symbol	Value
Disk:		
	$N_d{}^*$	46000
	M_d	$5.6 \times 10^{10}\ M_\odot$
	R_d	3.5 kpc
	z_d	245 pc
	$Q_\odot$	1.5
	$R_\odot$	8.5 kpc
	ϵ	70 pc
Bulge:		
	M_b	$1.87 \times 10^{10}\ M_\odot$
	a_b	525 pc
Halo:		
	M_h	$7.84 \times 10^{11}\ M_\odot$
	γ	3.5 kpc
	r_c	84 kpc

* The number of particles used for the disk.

Table 2. The parameters of the subhalos

Model	Number of subhalos	a [kpc]	$M_{\rm high}$ [$M_\odot$]	$M_{\rm low}$ [$M_\odot$]	$n_{\rm sub}{}^*$
point-mass models with $\beta = 0$					
A	784	70	10^8	10^8	
B	784	140	10^8	10^8	
C	392	140	2×10^8	2×10^8	
D	261	140	3×10^8	3×10^8	
E	200	175	4×10^8	4×10^8	
F	318	87.5	10^9	10^8	
G	313	280	10^9	10^8	
H	175	140	10^{10}	10^8	
I	1141	175	10^{10}	10^7	
J	1959	140	10^9	10^7	
extended-mass models with $\beta = 0$					
K	318	87.5	10^9	10^8	182
L	175	140	10^{10}	10^8	182
M	362	24.5	10^9	10^8	182
N	200	175	4×10^8	4×10^8	182
O	112	70	7×10^8	7×10^8	182
P†	280	52.5	10^{10}	10^8	170
Q	173	24.5	10^{10}	10^8	170
point-mass models with $\beta = 0.5$					
R	197	140	10^{10}	10^8	
S	362	87.5	10^9	10^8	
T	249	140	3×10^9	10^8	
U	361	157.5	10^9	10^8	

* The number of particles used for each subhalo.
† Only in this model, the total mass of the subhalo system is 13 % of that of the host galaxy.